

Tokamak Edge Model Validation and Improvement

D P Coster[†], J W Kim[†], Y Nishimura[†], R Schneider[‡],
X Bonnin[‡], V Rozhansky[¶] and S Voskoboinikov[¶]

[†] Max-Planck-Institut für Plasmaphysik, EURATOM Association, D-85748 Garching, Germany

[‡] Max-Planck-Institut für Plasmaphysik, EURATOM Association, D-17491 Greifswald, Germany

[¶] St. Petersburg State Technical University, 195251 St. Petersburg, Russia

E-mail: David.Coster@ipp.mpg.de

Abstract. Because of the complexity of the physics in the edge of divertor tokamaks, extrapolation from present day machines to future reactor or reactor-type devices is done using 2d-edge codes. The assumptions in the present codes are discussed with reference to running machines together with their relevance for extrapolation. The validity of the assumptions are tested by comparison of code results to experimental measurements on present machines. Issues relating to the remaining uncertainties are discussed, and some approaches to reducing these uncertainties are presented.

Submitted to: *Plasma Phys. Control. Fusion*

1. Introduction

The physics in the edge region of tokamaks (and stellarators) is complicated: the profiles of temperature and density in the Scrape-Off Layer (SOL) are determined by a competition between parallel and perpendicular (usually enhanced by anomalous processes) transport, as well as sources of particles and sinks of energy which arise from the interactions of the plasma with material surfaces (first wall, divertor plates). Aspects of this physics have been captured in 2d-edge codes (3d-codes are also in development for non-axisymmetric devices), and these codes are being used to make extrapolations from existing devices to proposed reactor scale devices.

The issue of the anomalous radial transport is important, but has been addressed elsewhere [1, 2, 3, 4]. In this paper we address some issues that arise in interpreting present experiments and in making predictions for future machines.

First, the issue of kinetic corrections, and the use of upstream data *versus* downstream data is discussed. Then some aspects related to target power asymmetries is addressed, including the effects of Edge Localised Modes (ELMs). Finally some issues related to the modelling of pumping, compression and enrichment are covered.

2. Upstream *versus* downstream

Two approaches are possible when analysing the edge plasma: to start with good target data and essentially to work upstream from there, or to start from good upstream measurements and work towards the target. Both have advantages and disadvantages, and which is used on a particular machine is often determined more by what's available than which would be "best". Ideally, of course, one would like to have both good upstream and downstream measurements, but this is often not the case.

If we consider ASDEX Upgrade (AUG) and JET [5], we find that AUG has good upstream measurements of electron temperature (edge Thomson system) and electron density (edge Thomson system and Lithium beam), but the target Langmuir probe data was often difficult to interpret, probably because of the very small angle of incidence to the flush mounted probes. JET, on the other hand, has a good target Langmuir probe system, but the measurement of upstream electron density and temperature profiles was often constrained by instrumental resolution issues.

Good upstream temperature and density profiles can very effectively determine the anomalous radial diffusivities, but the exact position of the separatrix is often in doubt as this comes from a fitting of an equilibrium to magnetic measurements and the mapping of the measured densities and temperatures to this equilibrium. If the same diagnostic is used to measure density and temperature, the position of the separatrix can also be well fitted as part of the procedure to calculate the transport coefficients.

The target densities and temperatures are not always that sensitive to changes in the radial anomalous transport coefficients, but are often a very sensitive function of the upstream density. An additional problem arises when using target profiles in a low collisionality plasma because the (fluid) codes used usually include a “flux limit” factor to account for kinetic effects, and the exact value chosen can often have an impact.

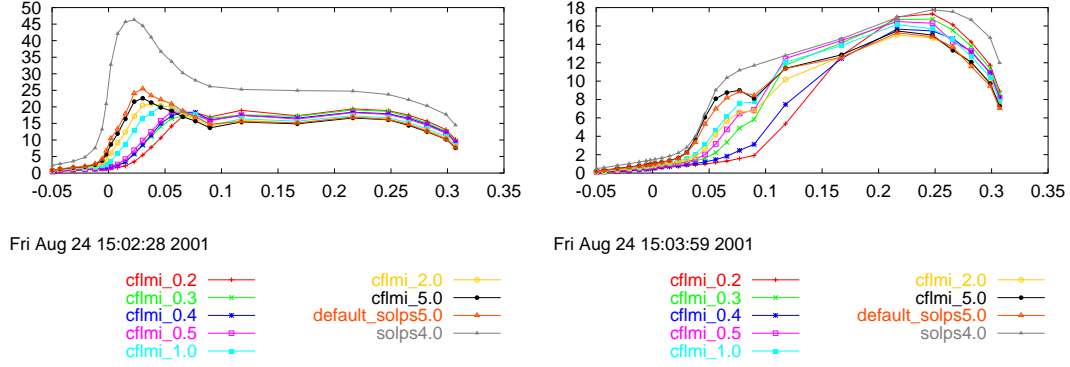


Figure 1. Effect of flux limits. D+C+He SOLPS5.0 B2-Eirene [6, 7] calculations for JET.

Figure 1 shows the predicted target temperatures for two different density cases on JET. In each case only the ion temperature flux limit was varied. For the lower density case, a wide range of plasma conditions is seen, and the “real” solution is probably somewhere in there. Trying to predict the radial transport from these measurements using a fixed “flux limit” would produce a range of values. For the higher density case, the situation is somewhat better.

AUG has recently replaced its DivII configuration with one that allows for a wider range of triangularity, but at the cost of a somewhat larger angle of incidence which should make the Langmuir probe interpretation easier. Operational changes and some hardware upgrades at JET should improve the spatial resolution of the upstream measurement. In the near future measurements on both machines should allow one to get a better idea of kinetic effects and allow the “flux limit” factor to be determined experimentally. Additional kinetic modelling would also be of use.

3. Target power asymmetries

Experimentally a power asymmetry is seen between the inner and outer divertors which is often not quantitatively reproduced by the codes.

In the codes the asymmetry is driven by:

- (i) the larger cross-sectional area on the outside ($\approx \frac{1+\epsilon}{1-\epsilon}$);

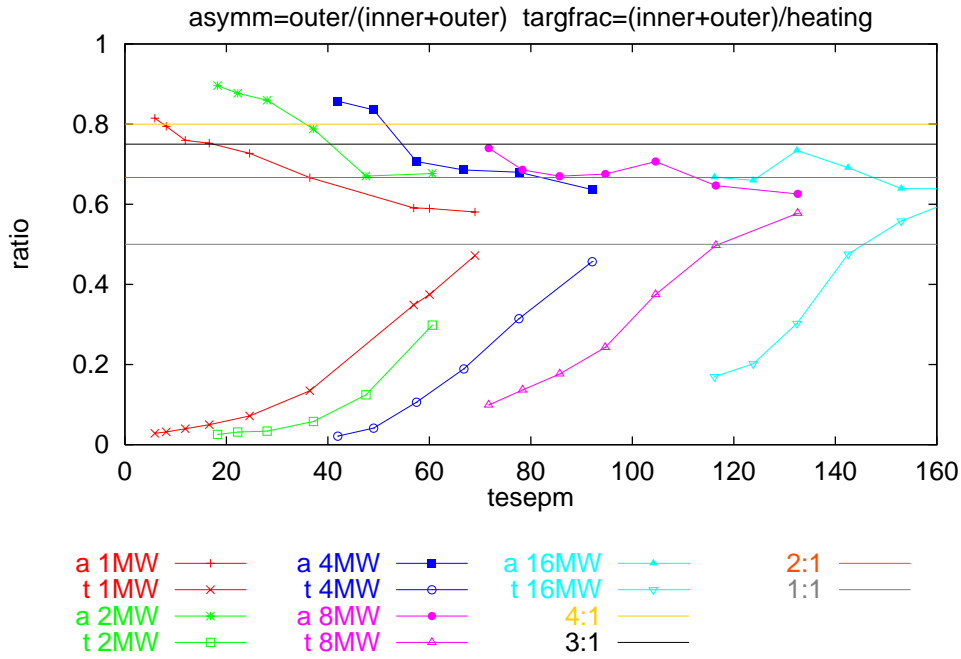


Figure 2. In/out power asymmetries. D+C+He SOLPS4.0 B2-Eirene [8, 9, 10] calculations for AUG.

- (ii) if the transport is assumed to be constant in real space, the flux surfaces are closer together on the outside (Shafranov shift), and hence the radial transport is larger there;
- (iii) a possible ballooning of the transport coefficients on the outside;
- (iv) diamagnetic and $\vec{E} \times \vec{B}$ drifts;
- (v) geometric effects arising from the targets themselves; and
- (vi) an amplification effect arising from differing plasma conditions near the targets.

On closed field lines at high enough temperatures, parallel transport is large enough to wipe out any temperature variation that might be driven by any of these effects. Thus the effects are likely to be strongest for higher densities, lower temperatures (*i.e.* higher collisionalities).

Figure 2 shows the predicted asymmetries in power reaching the target for B2-Eirene calculations of AUG plasmas with impurities but without drifts. Constant (in real space) transport coefficients were used. Thus these asymmetries arise from all the mentioned causes except drifts and ballooning.

During ELM events, a higher degree of in-out symmetry is seen experimentally, and it would be expected in the code output as well if the collisionality drops during an ELM event.

Figure 3 shows the predictions of SOLPS 5.0 B2 stand-alone calculations for three different sizes of ELM, for a range of densities. During the ELM event itself, for the

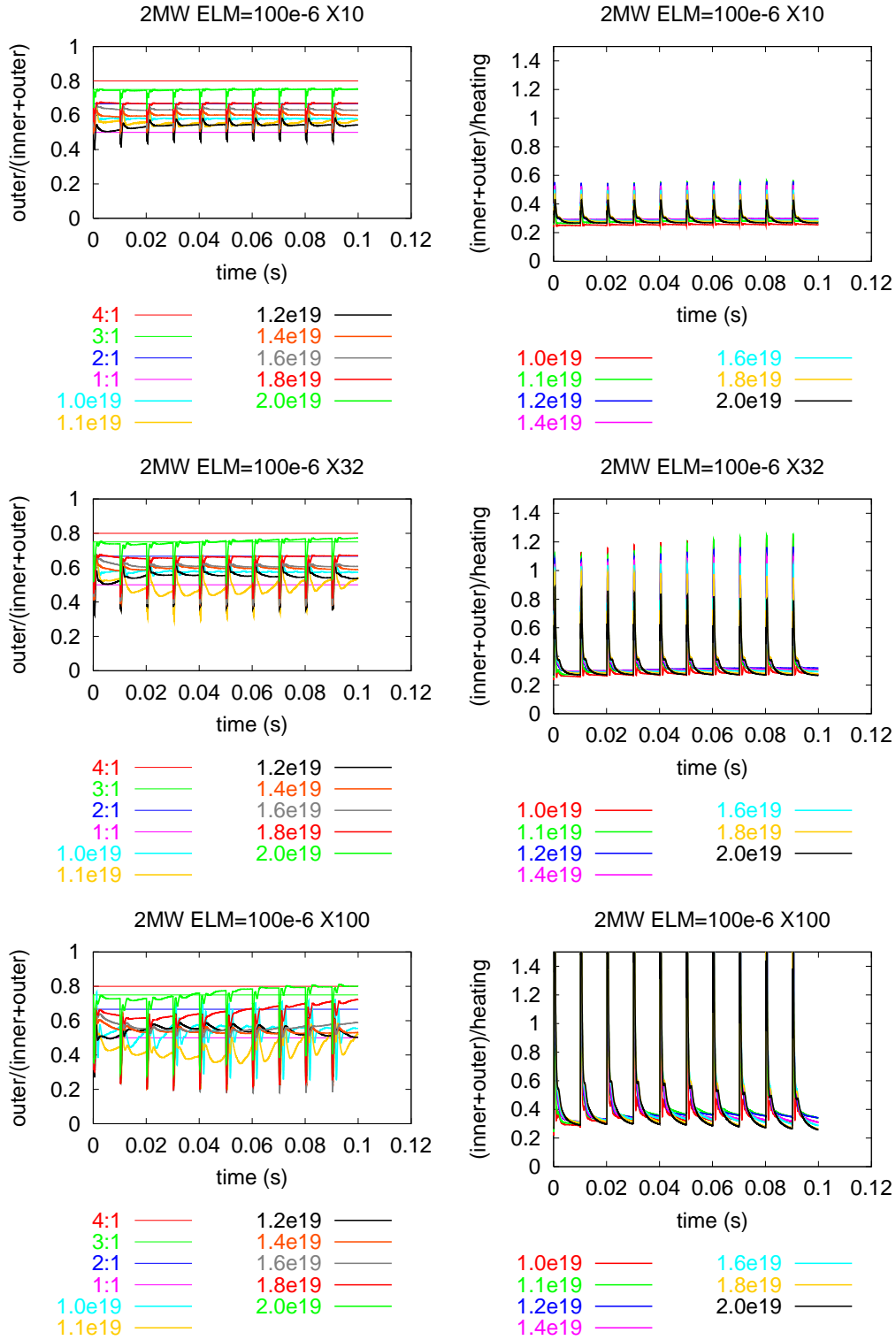


Figure 3. In/out power asymmetries. D+C SOLPS5.0 B2 [11] calculations for ELMs on AUG. Left, the ratio of power to the outer target to the total power to both targets. Right, the ratio of power to both targets to the average input power. From top to bottom the size of the ELM is varied by increasing the anomalous radial; transport coefficients used to produce the ELM ($\times 10$, $\times 32$ and $\times 100$ the steady state value).

higher density case a clear increase in the symmetry is seen. The calculations were started from converged steady state solutions, and changes can still be seen after 10 ELMs.

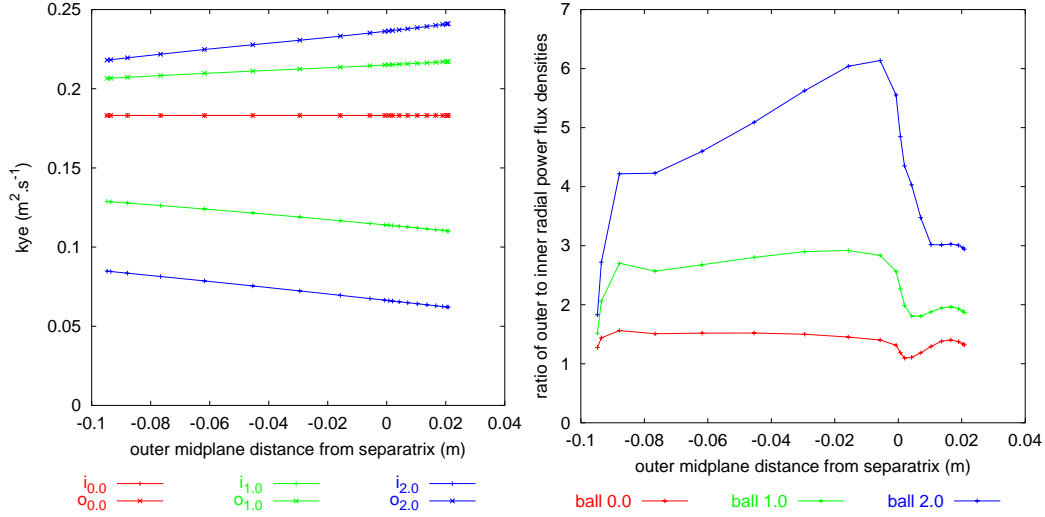


Figure 4. Left, the anomalous radial electron diffusivity on the inner and outer mid-planes (mapped to the outer mid-plane) for three ballooning factors. Right, the ratio of the radial power flux densities on the outboard side to the inboard side.

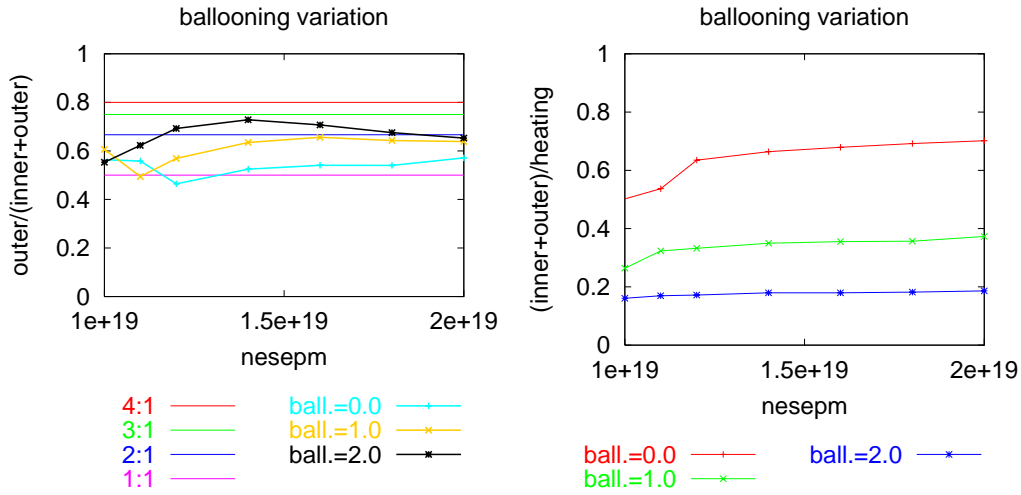


Figure 5. In/out power asymmetries. D+C SOLPS5.0 B2 calculations for AUG with differing degrees of transport ballooning. Left, the ratio of power to the outer target to the total power to both targets. Right, the ratio of power to both targets to the average input power.

An assumed ballooning of the anomalous radial transport coefficients, figure 4, has two effects. It tends to increase the power on the outboard side (an effect that, on closed field lines and at higher temperatures, is mitigated by parallel transport equilibrating the temperature on the flux surface. It also increases the radial transport in the SOL on

the outboard side in comparison to the inboard side, increasing the amount of energy lost (in the simulation) to the outer boundary, figure 5. One difficulty of doing calculations for looking at the ballooning effect is the determination of what quantities to hold fixed.

The issue of the effects of drifts has not been addressed in this paper: previous work [6, 12, 13] mostly with pure H or D plasmas because of the difficulties in getting convergence with both impurities and drifts) has shown that with ion diamagnetic drifts towards the X-point, the outer target becomes even hotter and the inner target even colder than the case without drifts, but that the plasma becomes more symmetric (or that the inner target can become hotter than the outer) when the drift direction is reversed. It is hoped that a more systematic study can be done in the future including both impurities and drifts.

4. Geometry effects, pumping

In previously reported work [14], the results of simulations of pumping and helium compression and enrichment were reported, and it was noted that the compression of both helium and hydrogen was reduced for the new DivIIb design compared to the older DivII design (which was optimised for power handling and pumping, at the cost of constraining the range of triangularities for which the plasma fitted into the divertor). The geometries are shown in figure 6.

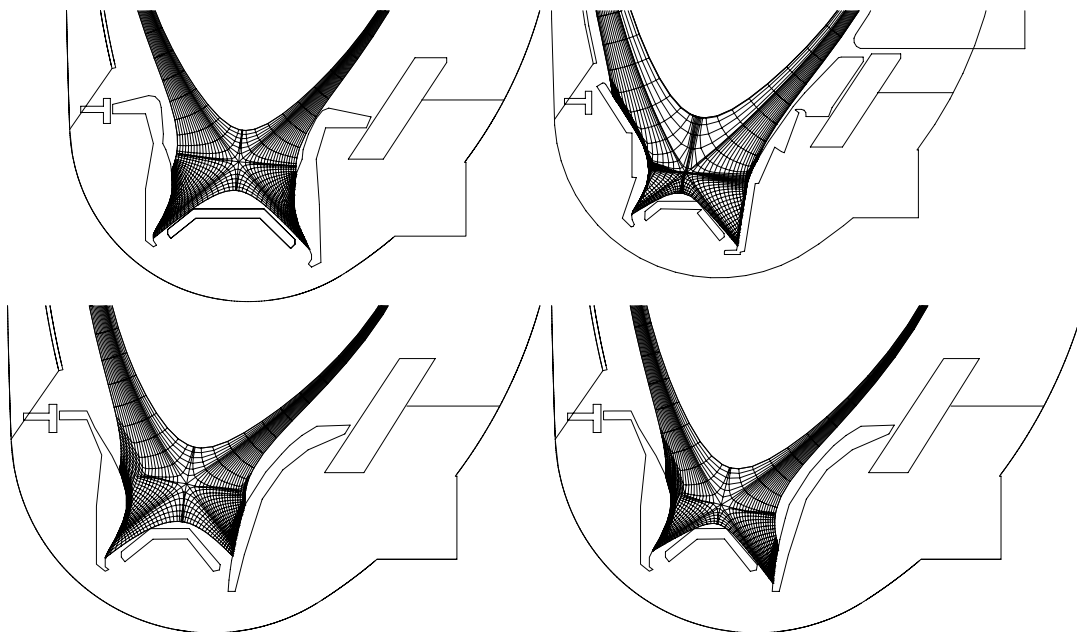


Figure 6. Counter-clockwise from top left: the old Divertor II configurations, two DivIIb configurations used in the design (“11302” and “11306”) and the final DivIIb design.

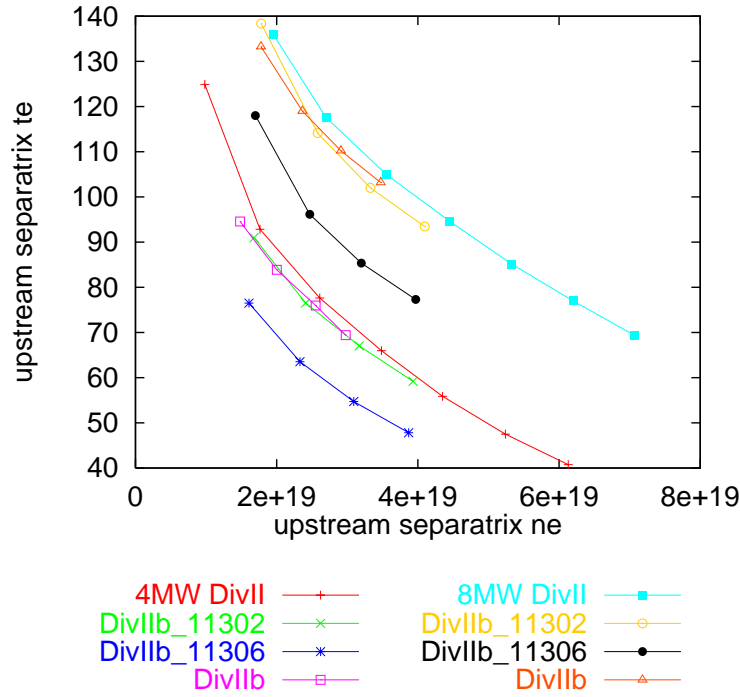


Figure 7. Upstream separatrix electron temperature *versus* density for 4 and 8 MW input power, for DivII, two DivIIb variants that were used for designing DivIIb, and the final DivIIb design. All simulations used the same transport coefficients.

The plasma conditions themselves are little changed. Figure 7 shows the calculated upstream separatrix temperature as a function of the upstream separatrix densities for a DivII case, two plasma conditions used in the design study, and a DivIIb case.

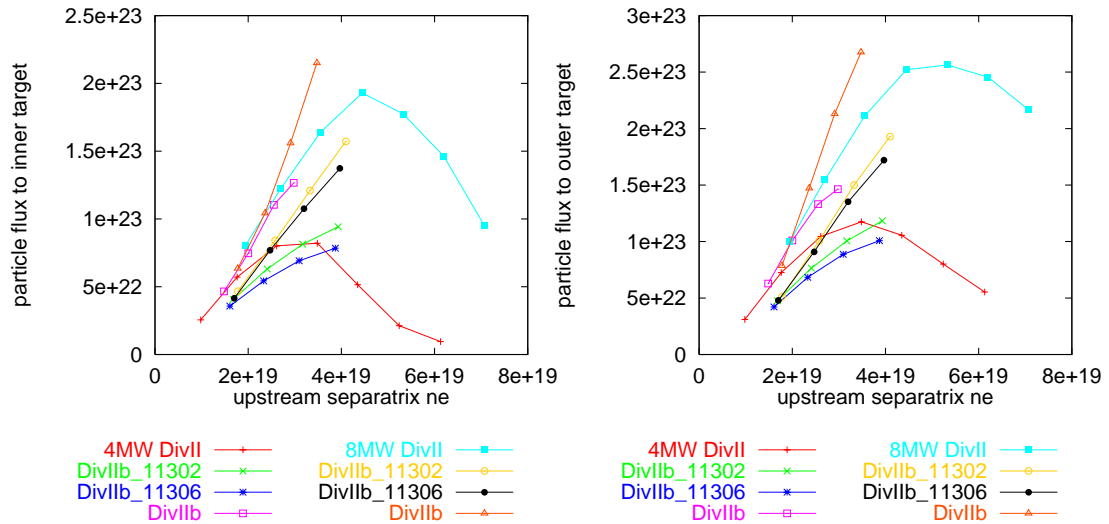


Figure 8. Inner and outer target fluxes *versus* upstream separatrix electron density for the same simulations shown in figure 7.

Figure 8 shows the fluxes to the inner and outer targets for the same conditions.

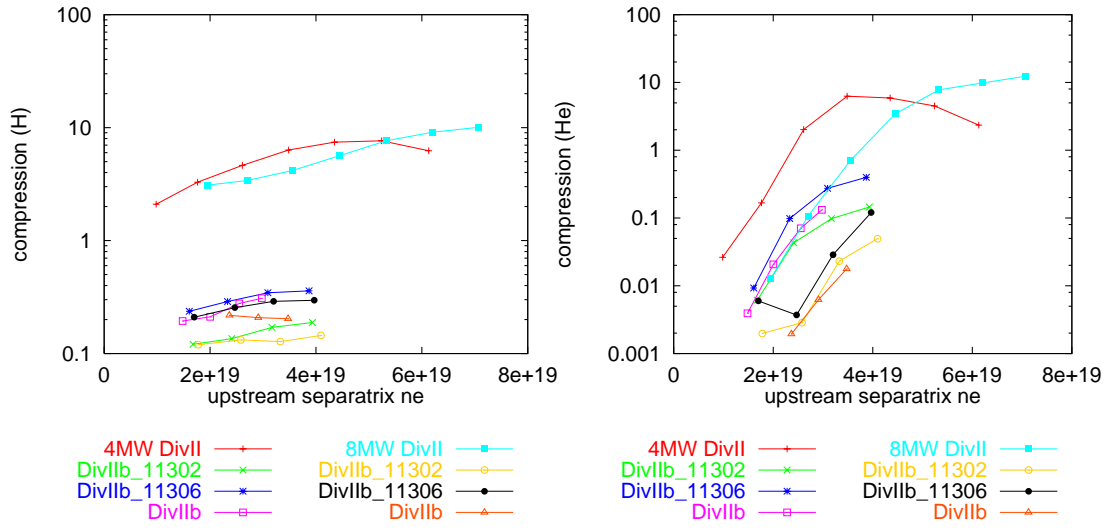


Figure 9. H and He compressions *versus* upstream separatrix electron density for the same simulations shown in figure 7.

The big difference is seen in the compressions, both for hydrogen and helium, figure 9. The enrichment predictions, figure 10 are, on the other hand, very similar.

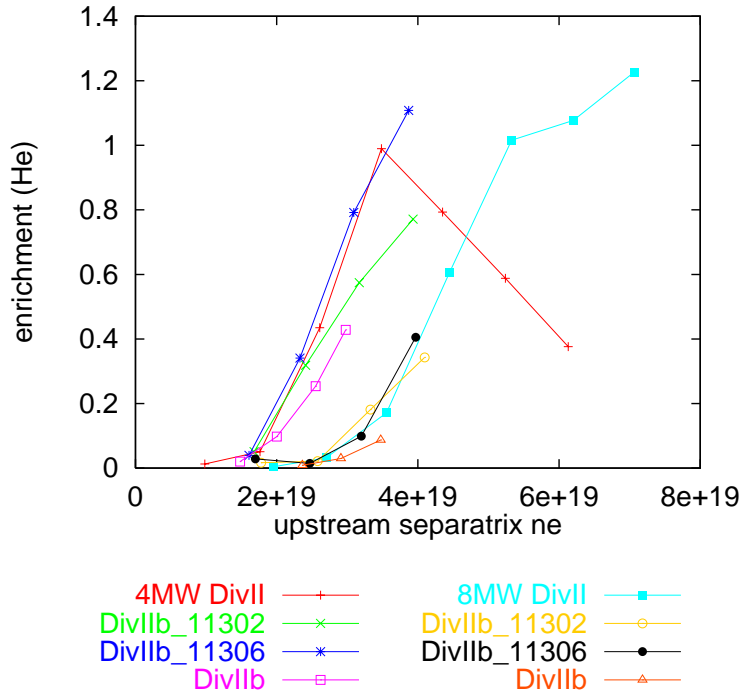


Figure 10. He enrichment *versus* upstream separatrix electron density for the same simulations shown in figure 7.

The code predicts a much lower flux into the dome region for the DivIIb case than for the DivII case, and this then causes a much lower predicted flux density of particles in both the dome region and in the pumping chamber. The helium enrichment, being

the ratio of the helium and hydrogen compressions, is unaffected by this. The data for similar cases are shown in table 1.

case	DivII	DivIIb_11302	DivIIb_11306	DivIIb
flux to inner target	1.3451E+04	1.3316E+04	1.1276E+04	1.7100E+04
flux to outer target	1.9213E+04	1.6424E+04	1.4516E+04	2.1043E+04
inner net	2.7156E+03	1.3090E+03	7.5332E+02	6.1841E+02
inner directed	3.7758E+04	7.0917E+03	9.5251E+03	8.1500E+03
outer net	6.1942E+02	-5.9043E+02	1.2306E+02	-6.1605E+02
outer directed	5.7930E+04	1.0650E+04	1.0853E+04	7.4321E+03
pump net	-3.3435E+03	-6.3778E+02	-8.1452E+02	-8.3371E+02
pump directed	5.9969E+04	1.6367E+04	1.9067E+04	1.4588E+04
dome directed	4.3376E+04	7.4171E+03	8.4032E+03	9.6187E+03
plenum directed	3.5913E+04	6.4100E+03	8.7407E+03	8.2160E+03
pumped	3.3500E+03	6.4100E+02	8.0100E+02	8.3800E+02

Table 1. Comparison of fluxes for DivII and DivIIb. A DivII case is compared to the two DivIIb variants used for design and the final DivIIb (see figure 6 for the geometries). The first two rows are the total plasma fluxes to the inner and outer targets (all fluxes in A). Next are the net and directed fluxes from the inner target into the dome region, the net and directed fluxes from the outer target into the dome region, and the net and directed fluxes from the pump chamber into the dome region. The “dome directed” and “plenum directed” are directed fluxes onto two (equal area) test surfaces under the dome and in the pumping plenum, respectively. The last row gives the flux of particles actually pumped in the simulation.

case	Inner Target		Outer Target	
	DivII	DivIIb	DivII	DivIIb
Incident flux				
H^+	1.3202E+04	1.6787E+04	1.8825E+04	2.0652E+04
H	1.7795E+04	1.1577E+04	1.9837E+04	1.3307E+04
H_2	4.9597E+04	7.0616E+03	4.0690E+04	3.3010E+03

Table 2. Comparison of incident hydrogen fluxes (in A) for DivII and DivIIb.

The explanation for this effect can be found by examining the fluxes to the target in detail, and this is done in table 2. While the H^+ fluxes are similar for both divertors (slightly higher in this case for DivIIb), as is the neutral hydrogen atom flux (slightly lower in this case for DivIIb), the molecular hydrogen flux is much reduced for DivIIb. Figure 11 shows that for DivII we have a drop in flux close to the separatrix with rising density and a movement of the flux maximum away from the separatrix. This feature of “preferential separatrix detachment” is lost in the DivIIb configuration with an uniform increase in the flux density. This is also seen in the electron density profiles, figure 12. The “preferential separatrix detachment” for DivII allows the escape of neutral particles from the plasma and their entry to the dome and pump regions. For DivIIb,

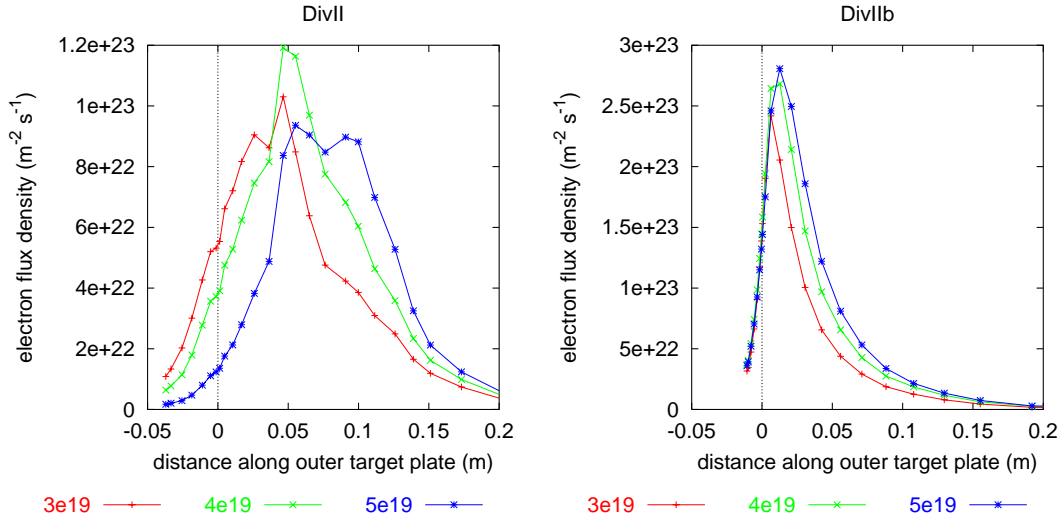


Figure 11. Electron densities at outer target for DivII and DivIIb.

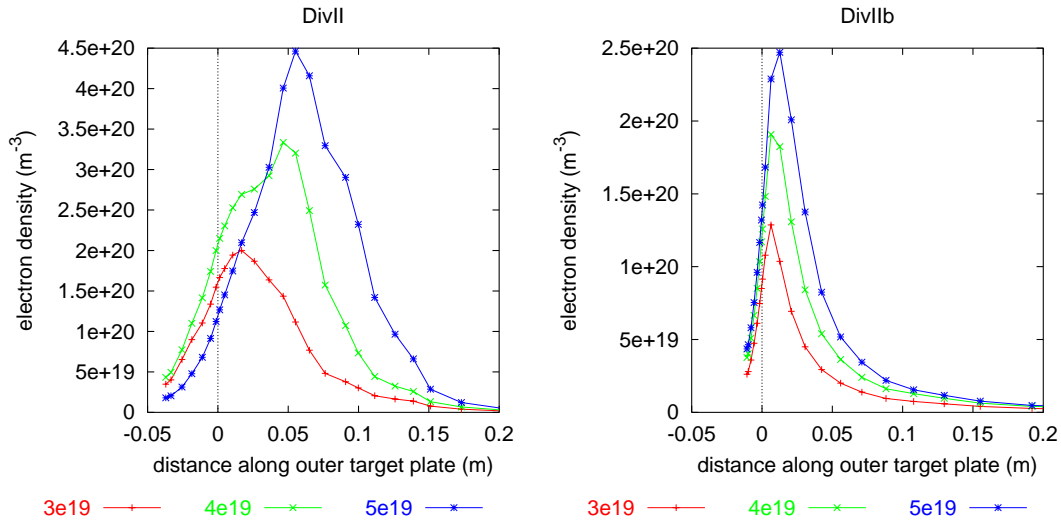


Figure 12. H^+ flux densities to the outer target for DivII and DivIIb.

the disappearance of this feature means that a higher fraction of the neutral particles are re-ionised in the plasma before they escape.

5. Summary

The present 2d-edge codes provide a valuable guide to the physics in the edge region of present machines and can provide a basis for the extrapolation to future devices. Care should be taken in comparing data from different machines gathered on different bases (upstream *versus* downstream). The effects driving in/out target power asymmetries are demonstrated, but the full calculation including the effects of ballooning, impurities,

drifts and ELMs still remains to be done. Some differences between two versions of the AUG divertor (DivII and DivIIb) related to pumping, compression and helium enrichment are also explored.

- [1] D. Coster, J. Kim, G. Haas, B. Kurzan, H. Murmann, et al., *Contrib. Plasma Phys.* 40 (2000) 334.
- [2] J.-W. Kim, D. P. Coster, J. Neuhauser, R. Schneider, and ASDEX Upgrade Team, *J. Nucl. Mater.* 290–293 (2001) 644.
- [3] D. Coster, X. Bonnin, K. Borrass, H.-S. Bosch, B. Braams, et al., in *Plasma Physics and Controlled Nuclear Fusion Research ...*, volume 0, pages –, Vienna, 2000, IAEA.
- [4] Y. Nishimura, D. P. Coster, J. W. Kim, and B. D. Scott, ASDEX Upgrade Edge Transport Studies by Turbulence and Braginskii Divertor Transport Codes, presented at PET, 2001.
- [5] D. Coster, G. Corrigan, M. Beurskens, K. Erents, W. Fundamenski, et al., in *28th European Physical Society Conference on Controlled Fusion and Plasma Physics, Funchal, Madeira*, 2001.
- [6] R. Schneider, D. Coster, B. Braams, P. Xantopoulos, V. Rozhansky, et al., *Contrib. Plasma Phys.* 40 (2000) 328.
- [7] V. Rozhansky, S. Voskoboinikov, E. Kaveeva, D. Coster, and R. Schneider, *Nuclear Fusion* 41 (2001) 387.
- [8] B. J. Braams, *Computational Studies in Tokamak Equilibrium and Transport*, PhD thesis, Rijksuniversiteit, Utrecht, Nederland., 1986.
- [9] D. Reiter, *Journal of Nuclear Materials* 196–198 (1992) 80.
- [10] D. Reiter, P. Boerner, B. Kueppers, M. Baelmans, and G. Maddison, Technical Report 428/90-8/FU-D, NET, EURATOM, 1990.
- [11] B. Braams et al., *Contrib. Plasma Phys.* 36 (1996) 276.
- [12] A. Chankin, J. Coad, G. Corrigan, S. Davies, S. Erents, et al., *Contrib. Plasma Phys.* 40 (2000) 288.
- [13] M. Rensink, S. Allen, G. Porter, and T. Rognlien, *Contrib. Plasma Phys.* 40 (2000) 302.
- [14] D. Coster, H.-S. Bosch, W. Ullrich, and ASDEX Upgrade Team, *J. Nucl. Mater.* 290–293 (2001) 845.